
# Development and biological evaluation of *p*NIPAM-based nanogels as vaccine carriers

María Laura Soriano Pérez, Javier Alejandro Funes, Carolina Flores, Luis Exequiel Ibarra, Marina Andrea Forrellad, Oscar Taboga, Laura Noelia Cariddi, Facundo Salinas, Hugo Héctor Ortega, Fabrisio Alustiza, Maria Molina

PII: S0378-5173(22)00990-5
DOI: https://doi.org/10.1016/j.ijpharm.2022.122435
Reference: IJP 122435

To appear in: *International Journal of Pharmaceutics*

Received Date: 5 July 2022
Revised Date: 14 November 2022
Accepted Date: 19 November 2022

Please cite this article as: M. Laura Soriano Pérez, J. Alejandro Funes, C. Flores, L. Exequiel Ibarra, M. Andrea Forrellad, O. Taboga, L. Noelia Cariddi, F. Salinas, H. Héctor Ortega, F. Alustiza, M. Molina, Development and biological evaluation of *p*NIPAM-based nanogels as vaccine carriers, *International Journal of Pharmaceutics* (2022), doi: https://doi.org/10.1016/j.ijpharm.2022.122435

# Development and biological evaluation of *p*NIPAM-based nanogels as vaccine carriers

María Laura Soriano Pérez [1], Javier Alejandro Funes [1], Carolina Flores[6], Luis Exequiel Ibarra [2], Marina Andrea Forrellad [3], Oscar Taboga [3], Laura Noelia Cariddi [4], Facundo Salinas [5], Hugo Héctor Ortega [5], Fabrisio Alustiza [1], Maria Molina [5].

[1] Grupo de Sanidad Animal, INTA Marcos Juárez. Córdoba, Argentina

[2] Consejo Nacional de Investigaciones Científicas y Técnicas (CONICET), Instituto de Biotecnología Ambiental y Salud (INBIAS), Río Cuarto, 5800, Córdoba, Argentina

[3] Instituto de Agrobiotecnología y Biología Molecular (IABIMO), INTA-CONICET. Hurlingham, Buenos Aires, Argentina

[4] IITEMA CONICET-UNRC. Río Cuarto, Córdoba, Argentina

[5] CMC, ICIVET-Litoral, UNL-CONICET. Esperanza, Argentina

[6] INCIVET CONICET-UNRC. Rio Cuarto, Argentina

## Abstract

"Smart" nanogels are an attractive tool for the development of new strategies of immunization in veterinary medicine. Here, we reported the synthesis and physicochemical characterization of thermoresponsive nanogels based on poly(N-isopropylacrylamide) (*p*NIPAM) and their *in vitro*, *ex vivo,* and *in vivo* (mice model) performance. Smart nanogels of ca. 250 nm, with a transition temperature of 32°C were obtained by precipitation polymerization. Assays to evaluate *p*NIPAM nanogels cytotoxicity were performed in different cell lines showing high biocompatibility (>70%). The efficient internalization of the system was studied by confocal microscopy as well as flow cytometry. The ability to protect and deliver antigens was analyzed using the outer membrane lipoprotein A (OmlA), an important virulence factor of *Actinobacillus pleuropneumoniae* (*App)* cause of porcine pleuropneumonia. This lipoprotein was synthesized by recombinant technology and its technique was also described. The biodistribution of *p*NIPAM nanogels administered intranasally was performed *in vivo* and *ex vivo* through Pearl Imaging System, which showed that nanogels were kept mostly in the lungs during the evaluated time. Besides, the efficacy of the proposal nanogel-based vaccine was studied *in vivo* by measuring the antibody titers of BALB/c mice inoculated with OmlA encapsulated into *p*NIPAM nanogels compared to OmlA plus aluminum hydroxide adjuvant. The results proved the ability of nanogels

to stimulate a humoral immune response. Therefore, we have demonstrated that *p*NIPAM nanogels can be used as an efficient platform for vaccine nanocarriers.

**Keywords**: *p*NIPAM nanogels, vaccine carrier, animal model, macrophages cells

## 1. Introduction

Polymeric hydrogels, especially nanoscale hydrogels, are an attractive class of materials with wide potential for different applications in the field of veterinary medicine (Carvalho et al., 2020). Nanogels are cross-linked polymeric networks capable of absorbing large quantities of water and biological fluids without dissolving. Among their main physicochemical and biological properties, nanogels have a large contact surface, high loading capacity, versatility in shape and size, and excellent biocompatibility (Neamtu et al., 2017). Due to these characteristics, nanogels can swell in aqueous mediums and encapsulate water-soluble therapeutics biomolecules, proteins, or nucleic acids, which finally will be loaded into the polymer matrix (Chacko et al., 2012). To ensure animal health and welfare, immunization is one of the main practices applied in veterinary medicine, so the investigations of non-invasive and effective vaccination strategies become a new area of development. Therefore, based on their ability to carry and protect vaccine antigens by avoiding their degradation, nanogels emerge as one of the most promising technology in the field of animal vaccination (Hernández-Adame et al., 2019). Thus, the possibility of using these materials with subunit vaccines in innovative immunoprophylactic preparations would replace the classical inactivated whole cell preparations currently employed in veterinary or would allow the use of adjuvant-free vaccines. Several reports have shown the protective efficacy of similar subunit-based vaccine formulations with nanogels in mice and other species. (Debache et al., 2011; Nochi et al., 2010; Yang et al., 2017). For example, the article published by Yang et al. in 2017 demonstrated that the use of nanogel as an adjuvant enhanced the protective efficacy of the influenza vaccine in mice. In this work, the highest survival rate was found in a group of mice immunized with nanogel plus vaccine antigen compared to the group of vaccine antigen alone or vaccine antigen plus alum. These survival rates were obtained 14 days post-challenge with a lethal dose of the pandemic influenza A virus. Another advantage of nanoparticles is the efficient uptake and acceptance by mammalian cells as a requirement to achieve immunization (Pippa et al., 2021; Wibowo et al., 2021).

"Smart" nanogels can respond to a variety of environmental stimuli such as pH, temperature, ionic strength, or electric field through a conformational change, i.e. swelling/shrinkage, disaggregation, etc (Molina et al., 2015; Preman et al., 2020). Nanogels based on the

thermoresponsive polymer *poly* N-Isopropylacrylamide (*p*NIPAM) have a lower critical solution temperature (LCST) around 32°C and therefore higher temperatures trigger conformational changes resulting in water loss, an increase of hydrophobicity, and volume collapse (Boutris et al., 1997; Chalal et al., 2010; Tang et al., 2021; Tokuhiro et al., 1991). This special feature is very attractive for biological applications due to the proximity of LCST to the physiological temperature of mammals. It is also important to mention that, despite this, it is necessary to know the potential of *p*NIPAM nanogels as an antigen delivery system. An interesting animal model disease to assay *p*NIPAM nanogels as an antigen delivery system, is the outer membrane lipoprotein A (OmlA), an important virulence factor of *Actinobacillus pleuropneumoniae* (*App)*, the cause of porcine pleuropneumonia with important economic loss in the pig industry worldwide (Gottschalk, 2012), and could be an interesting antigen candidate to incorporate into nanogels-based vaccines (Alcón et al. 2006; Alcón et al. 2003; Alcón et. al 2005). Although there are a few available vaccines for this disease, most of them use inactivated whole *App* cells and their protective efficacy is debated (Loera-Muro and Angulo, 2018). Within preliminary evaluations of vaccine candidates, the use of antigen-presenting cells (APC) in the assays with *p*NIPAM-based nanogels will allow us to elucidate the first step of antigen processing and the immune response generated.

The main objective of this work was the development of *p*NIPAM-based nanogels as vaccine nanocarriers of OmlA and its biological evaluation. We described the effect of *p*NIPAM nanogels in macrophages (RAW 264.7 cell line) using *in vitro* cytotoxicity tests and uptake assays. The ability of nanogels to encapsulate and control the release of OmlA antigen was demonstrated. Moreover, the biodistribution of *p*NIPAM nanogels after intranasal instillation and the *in vivo* humoral immune response were performed in mice administered with formulations, using OmlA encapsulated into *p*NIPAM-based nanogels.

## 2. Materials and Methods

### 2.1. *p*NIPAM nanogels

#### 2.1.1. Materials

For nanogels synthesis, N-isopropylacrylamide (NIPAM, 100%), allylamine, and acrylic acid (AA) monomers were purchased from Scientific Polymer Products. N,N-methylenebysacrylamide (BIS) from Sigma Aldrich was used as the cross-linker agent. Ammonium persulfate (APS, Cicarelli) was used as the initiator agent, and sodium dodecyl sulfate (SDS, Invitrogen™) as the stabilizer. For their observation in cell experiments, the nanogels were labeled with fluorescein isothiocyanate (FITC, Sigma) or ADS790WS IR dye (ADS Inc) using N', N'-dicyclohexyl carbodiimide (DCC) as coupling agent. Water was triply distilled. All reagents and solvents in this work were used as received and were of analytical quality.

#### 2.1.2. Synthesis of nanogels

Nanogels were synthesized via radical polymerization of NIPAM, using APS to initiate the reaction (Pelton and Chibante, 1986). The crosslinking agent BIS was added. Nanoparticles were made by the technique of precipitation polymerization with a low concentration of monomer (NIPAM) and high concentration of initiator (APS). The pre-gel solution was made as follows: NIPAM 123 mM, BIS 2.15 mM, SDS 1 mM dissolved in a final volume of 200 mL of distilled water. This solution was deoxygenated via nitrogen bubbling and then kept it stirring for 1 h at 70°C in a nitrogen environment. After that, an aqueous solution of APS (1.7 mM) was added and the reaction was carried out for 4 h under the same conditions (70°C, nitrogen environment, stirring). The nanogels were purified by dialysis (molecular weight cut off of 12 kDa, SIGMA) against distilled water for two weeks and the distilled water was completely replaced three times per day. Finally, nanogels were freeze-dried (LABCONCO Freezone Plus 6) and stored at room temperature until used. The synthesis was performed in triplicate.

#### 2.1.3. Dye labeled nanogels

Alternatively, modified nanogels were synthesized in order to label them with different dyes.

For green fluorescent *p*NIPAM nanogels, a co-monomer (allylamine, 3.34 mg) (5.85 mM) was incorporated into the initial reaction of 10 mL of distilled water (final volume) to obtain nanogels with free amine groups. This monomer allows the covalent incorporation of FITC into the thermoresponsive nanogels. Once the polymerization reaction ended, the pH was adjusted to 8 and kept on ice and darkness, followed by the addition of 1 mg of FITC (0.26 mM). Finally, labeled nanogels were dialyzed in a membrane tube against ethanol for two days to remove FITC excess, and then against distilled water until FITC was not detected in the outer solution by a spectrometer (280 nm). For near-infrared (NIR) fluorescent *p*NIPAM nanogels conjugates, acrylic acid as the co-monomer (3.34 mg) (4.64 mM) was incorporated to allow binding with ADS790WS IR dye via the carboxylic group. For this reaction 137 mg of NIPAM, 3.34 mg AA, 3.32 mg BIS, and 2.85 mg of SDS were used in 10 mL of distilled water. Once the synthesis was completed, 6.67 mg (3.23 mM) of DCC was added to allow coupling of 10 mg (1.19 mM) of ADS790WS in incubation overnight at 4° C. ADS790WS-nanogels were dialyzed in a dialysis tube against distilled water for two weeks in darkness. The synthesis was performed in triplicate.

### 2.2. *p*NIPAM nanogels characterization

#### 2.2.1. Dynamic Light Scattering (DLS)

The particle hydrodynamic diameter and polydispersity index (PDI) of the nanogels were measured at different temperatures using the Autosizer Malvern 4700. During the measurement

process, the size was measured following a temperature ramp ranging from 25°C to 40° C. For this purpose, a nanogel solution was prepared with a final concentration of 1 mg/mL in distilled water. Experiments were performed in triplicates and results were shown as the mean ± the standard deviation.

#### 2.2.2. Atomic Force Microscopy (AFM)

The topography of nanogels was scanned with AFM Agilent Technologies 5420 Scanning Probe® Microscope using non-contact mode. A drop of 1 mg/mL nanogel solution was placed onto a cleaned mica surface and dried at room temperature by air drying process before observation. Image analysis and measurements were performed using the Gwiddion software.

#### 2.2.3. Fourier Transform Infrared Spectroscopy (FT-IR)

The *p*NIPAM nanogels spectrum was acquired using KBr (potassium bromide) pellets in a wavenumber range of 600-4000 $cm^{-1}$ with a resolution accuracy of 4 $cm^{-1}$ using the spectrophotometer Nicolet Impact 400 at room temperature.

#### 2.2.4. Dye labeled nanogels

To characterize the dye conjugates, the emission fluorescence spectrum of the FITC-nanogels in water solution (1 mg/mL) was measured from 510 to 610 nm at an excitation wavelength of 495 nm using a SpexFluoromax spectrofluorometer.

For the same purpose, the optical properties of ADS790WS-nanogels were characterized in an aqueous solution (1 mg/mL) by a UV–vis spectrophotometer recording the absorption spectrum.

### 2.3. Recombinant protein outer Membrane Lipoprotein A (OmlA)

#### 2.3.1. Bacterial strain and growth conditions

The reference strain *App* serotype 1 ATCC 27088 was seeded on a 5% equine blood agar plate in an aerobic atmosphere at 37°C for 24 h. Then, a single pure colony was selected and inoculated into BHI (Brain heart infusion growth medium) broth containing 4 mg/mL β-NAD (β nicotinamide adenine dinucleotide) (Roche) and maintained overnight under stirring at 37°C.

#### 2.3.2. Molecular cloning of *omlA*

Genomic DNA from *App* serotype 1 was extracted by Genomic DNA Purification Kit (Fermentas®) according to the manufacturer's instructions. The gene (*omlA*) encoding an outer membrane lipoprotein A from *App* serotype 1 was amplified using the pair of primers: *omlA* Fw (AGGATCCAATATTGCAACAAAATTAATG) and *omlA* Rv (AGAATTCTTAGGTTGCCGTAGCACCGATTAC). PCR conditions consisted genomic DNA (50 ηg), 0.5 µM of each primer (FAGOS), 0.2 mM of each dNTP

(Promega), 1.5 µM of $MgCl_2$, 1X buffer (Buffer 5X GoTaq Promega) and 0.5 U GoTaq polymerase DNA (Promega) in a final volume of 25 µL. PCR was initiated with an incubation step at 94 °C for 5 min, followed by 35 cycles of 94 °C / 30 s, 58 °C / 30 s, and 72°C / 1 min 40 s with a final extension step at 72 °C for 10 min. The amplified DNA products *omlA* of 1032 bp were electrophoresed on a 0.8 % (w/v) agarose gel (Biodynamics®). Once identified, the PCR products were purified using a PCR purification kit (Qiagen, Hilden, Germany) according to the manufacturer´s protocols. DNA concentration and purity were recorded and *omlA* gene was cloned into pGEM-T Easy plasmid (Promega, Madison, WI). *E.coli* DH5α strain was transformed and white colonies, carrying the recombinant pGEM-T Easy:*omlA* vector, were selected on LB plates containing 100 µg/mL ampicillin and supplemented with 0.1 mM IPTG/ 0.05 mM Bluo-Gal. Subsequently, the *omlA* fragment was obtained with enzyme digestion (*BamH*I and *EcoR*I), purified through Kit Easy Pure Quick Gel Extraction (TransGen Biotech Co) and subcloned into the same restriction site in the expression pRSETa vector (which allows the expression of recombinant OmlA protein as 6XHis-tag fusion). Recombinant plasmid pRSETa::*omlA* from positive clones were transformed into *E. coli* BL21 (AI) for expression.

2.3.3.Expression and purification of OmlA

*E. coli* BL21 (AI) recombinant cells (pRSETa::*omlA*) were cultured into LB medium supplemented with glucose (0.1%) at 37°C until an $OD_{600nm}$ of 0.4-0.6 was reached. From this point, arabinose (0.2%) was added to induce the expression of OmlA during 3 h culture at 37°C. The bacteria were pelleted by centrifugation (6000 rpm) for 10 min at 4°C and suspended in Lysis buffer (LB) containing: Tris-HCl (pH 8) 50mM, NaCl 400 mM, KCl 100 mM, Glycerol 10%, and Tritón X100 1%. After a treatment with lysozyme (SIGMA) 1 mg/mL for 1 h at 4°C and DNAsa (SIGMA) 5µg/mL for 30 min at 4°C, the samples were homogenized using a mechanical disruptor (FastPrep®24, MP Biomedicals) with sterile glass beads (0.2 - 1 µm SIGMA). The disruption was performed in three cycles of 21 s at 600 rpm. Following, lysed cells were centrifuged at 6000 rpm for 20 min; the supernatant containing total proteins was recovered and centrifuged again at 13000 rpm for 40 min, 4°C. The last resulting supernatant, containing the fraction of soluble proteins, was kept. The OmlA-6X His-tagged protein was determined by SDS-PAGE and Western Blot analysis and purified by affinity chromatography using Ni-NTA agarose resin (QIAGEN, Germany).

2.3.4.Identification and Western-Blot analysis

The final samples were analyzed by sodium dodecyl sulfate-polyacrylamide gel electrophoresis (SDS-PAGE) and proteins were identified by Coomassie Blue R-250 staining. In parallel, the gel proteins were transferred to nitrocellulose membranes (Bio-Rad nitrocellulose membrane) to

identify the recombinant OmlA.His-tag by immunoblotting using, firstly, a mouse monoclonal antibody to His6-tagged proteins (Anti-His6, Roche®) and secondly, a goat antibody anti-mouse alkaline phosphatase conjugates (Sigma Aldrich®). BCIP/NBT (5-bromo-4-chloro-3-indolyl phosphate/*p*-nitroblue tetrazolium chloride) chromogen was used as a substrate in order to detect proteins of interest.

### 2.4. Encapsulation and Release Studies

To assess the loading capacity and efficiency of *p*NIPAM nanogels, two proteins were used. First, a common ovalbumin protein model (OVA) (chicken egg white albumin, Sigma Aldrich®) was used taking advantage of its similar molecular weight to OmlA. For this, 10 mg of nanogels with 10 mg of OVA were dissolved and incubated in 3 mL of PBS overnight at 4°C to allow swelling of the nanogels. The resulting solution was centrifuged in a centrifugal device Vivaspin 100 kDa (Sartorius AG, Göttingen, Germany) at 4°C (three times for 30 minutes at 6000 rpm). The quantification of non-encapsulated OVA was performed by BCA (Bicinchoninic Acid, Thermo Fisher Scientific™) protein assay in the filtered portion. The loading capacity and loading efficiency were calculated as follows:

$$Loading\ capacity = \frac{W_i - W_f}{W_{NG}}\, x\ 100\%$$

$$Loading\ efficiency = \frac{W_i - W_f}{W_i} x\ 100\%$$

where $W_i$ is the initial weight of OVA, $W_f$ is the final weight of OVA remaining in solution and $W_{NG}$ is the weight of nanogels used.

The release studies were performed by dialysis method against PBS for OVA. For this purpose, the resulting solution of nanogels loaded with OVA was transferred to a dialysis bag with a membrane of 50 kDa cutoff. These dialysis bags were placed in 10 mL of PBS at 37°C to evaluate the thermosensitive triggered release of nanogels. At certain times, aliquots of 200 μL were taken from the external solution and the concentration of OVA was determined by a BCA protein assay. After each measurement, the same volume was replaced with a fresh medium. Finally, the cumulative release was calculated at 37°C. Furthermore, the release studies were performed at 4°C to check the stability of the system. All assays were made in triplicate and results were shown as the mean ± the standard deviation.

In the case of OmlA, and considering the difficulties to obtain it, only an encapsulation and release study at 37 °C was performed in order to corroborate the model, following the same procedure described above.

The stability of OmlA after release was checked by SDS-PAGE. A sample of released OmlA and non-encapsulated OmlA solutions were seeded in a polyacrylamide gel to compare their electrophoretic profiles. Samples were separated by discontinuous SDS-PAGE with 4% stacking gel and 12% separating gel. Aliquots of solutions were mixed with equal volumes of sample buffer (2.5% SDS, 5% 2-mercaptoethanol, 25% glycerol, and 0.003% bromophenol blue in 0.05 M Tris hydrochloride [pH 6.8]) and boiled for 7 min before electrophoresis. The observation of the gels was performed by Coomassie brilliant blue R250 staining.

### 2.5. *In vitro* studies

#### 2.5.1.Cell Culture

Mouse macrophages (RAW 264.7 cell line) were cultured in Dulbecco´s Modified Eagle medium (DMEM) supplemented with 10% fetal bovine serum (FBS), streptomycin (10000 µg/mL), and amphotericin B (25 µg/mL). Cultures were maintained at 37 °C in a 5% $CO_2$ humidified incubator.

#### 2.5.2.Incorporation of Fluorescent Labeled Nanogels by Flow Cytometry (FC) Analysis

To evaluate the uptake of *p*NIPAM nanogels in macrophage cells, RAW 264.7 cells were seeded into 24-well microplates (Nunc, Denmark) at a concentration of 2 x $10^5$ cells/mL and then growing under the same protocol previously described. After 24 h of culture, cells were incubated with a FITC-nanogel solution in DMEM (0.01 mg/mL) previously swollen in the same medium for 12 h at 4° C. At four time points (3, 6, 12, and 24 h) the medium was removed, and cells were washed twice with PBS and trypsinized to obtain a cell suspension. Finally, cells were centrifuged and resuspended into 500 µL of PBS with 1% of FBS to be analyzed by FC (flow cytometry). The samples were analyzed in a Guava Easycyte 6 2L flow cytometer (Merck). The FITC-nanogels fluorescence was measured in the 523/30 nm detector. A total of 10,000 events were collected and histograms were made in the green-B-HLog channel (523/30 nm) for subsequent analysis and the calculation of the mean fluorescence intensity values (geometric mean) to compare the different treatments. The experiment was conducted in quadruplicate.

#### 2.5.3.Confocal microscopy

To visualize the uptake of nanogels by macrophages, RAW 246.7 cells were incubated with FITC-nanogels and observed by confocal microscopy. Thus, 2 x $10^5$ cells were cultured in cover slip placed on 6-well plates at 37 °C, 5% $CO_2$ in a humidified incubator. After 24 h, cells were treated with 0.01 mg/mL of FITC-nanogels in DMEM and kept under the same conditions for 16 h. After that, the culture medium was removed and cells were washed twice with PBS to remove non-internalized nanogels. Then, each monolayer of cells was covered with 500 µL per well of Hoechst 33342 solution (10 µg/µL) to label nuclei and then fixed with 2% paraformaldehyde. Mounting

was done using the cover slip on glass slides to finally, observe the fluorescence of FITC-nanogels and Hoechst 33342 into the cells with a Confocal Microscope (FV 1000 Olympus).

#### 2.5.4. MTT assay

This assay is based on the ability of viable cells to metabolize the MTT (3-(4,5-dimethylthiazol-2-yl)-2,5-diphenyltetrazolium bromide) dye to finally measure the optical density of formazan product by spectrophotometry.

For this protocol, 5000 cells per well were seeded in 96-well-plates (Nunc, Denmark) and after 24 h of incubation, the monolayer was treated with three concentrations of nanogels (0.0001, 0.01, and 1 mg/mL) for 24 h. To this end, dry nanogels were mixed with DMEM to obtain these three final solutions. Untreated cells served as negative control (100% viability). After nanogels exposure, each well was washed with PBS and 100 µL of MTT solution was added (in DMEM using 0.5 mg/mL) to incubate it at 37°C for 3 h in darkness. MTT solution was removed and 100 µL per well of DMSO was used to dissolve the formazan precipitate. Last, the plates were shaken and their optical density was measured at 540 nm. All experiments were made in triplicate.

#### 2.5.5. Cell Viability by FC Analysis

As a standard protocol, 1 x $10^5$ cells per well were seeded into 24-well-plates (Nunc, Denmark) and after 24 h incubation, cells were treated with three concentrations of nanogels (0.0001, 0.01, and 1 mg/mL). To this end, dry nanogels were mixed with DMEM to obtain these three final solutions and two exposure times were tested, including 6 and 24 h. After these periods, the medium containing nanogels was removed and cells were washed twice whit PBS. The monolayer was trypsinized, harvested, and suspended in 500 µL of a solution containing 1 µL of LIVE/DEAD™ Fixable Far Red and incubated for 20 min in dark. Finally, cells were centrifuged, resuspended in 500 µL of PBS with 1% of FBS, and analyzed using a Guava Easycyte 6 2L flow cytometer (Merck). The fluorescence emission was detected in the Red-R-HLog channel. Cells incubated in a complete culture medium served as lived control. These experiments were carried out in triplicate.

### 2.6. *In vivo* studies

#### 2.6.1. Biodistribution imaging of *p*NIPAM nanogels

##### 2.6.1.1. Imaging System and animals

To monitor the follow-up of nanogels via mucosal applied in small animals, Pearl® Trilogy Small Animal Imaging System was used. This non-invasive system capture *in vivo* and *ex vivo* images of 700 and 800 nanometer NIR fluorophores. The software Image Studio software V 5.2 was used for data capture and analysis. This determines arbitrary units for the quantification of the

fluorescence intensity (RFU: relative fluorescence units). All images were presented in pseudocolor because it can distinguish different intensities easier.

Adult female BALB/cCmedc mice (6-7 weeks) were housed in individually ventilated cage (IVC) systems (Allentown Inc., USA) and given food and water ad libitum. The temperature of the animal facility was 23 °C with a 12-h light/dark cycle.

All the procedures were carried out according to the Guide for the Care and Use of Laboratory Animals (NRC, 2011) and with the approval of the Institutional Ethics and Security Committee (Protocol Nº 632/20) of the School of Veterinary Science of the National University of Litoral, Santa Fe, Argentina. The Centre for Comparative Medicine is an entity compliant with GLP for conducting preclinical tests inspected by the Argentine Accreditation Organism (member of the OECD) and the certifications of local regulatory agencies like the ANMAT (National Argentine Administration of Drugs, Food, and Medical Technology,) and the SENASA (National Argentine Service of Animal Sanitation and Food Quality).

#### 2.6.1.2. Experiment and animal imaging

One group of five BALB/cCmedc mice was randomly selected and administered intranasally with ADS790WS-nanogels. 20µL (10 µL per nostril) of a 1.05 mg/mL solution of ADS790WS-nanogels in PBS were dropped in each mouse (1 mg/kg). During the study, animals were monitored and their physiological constants were registered. The animals were *in vivo* imaged on a Pearl® Trilogy Small Animal Imaging System at 30 min, 1, 2, 4, 8, 12, and 24 h after intranasal administration with ventral, lateral, and dorsal views. In addition, animals were imaged at zero time to establish a basal level of fluorescence. For all procedures, animals were induced and anesthetized with 5% and 2% Isoflurane, respectively. In parallel, animals were euthanized by anesthetic overdose at 1, 4, 8 h, (n= 1) and 24 h (n= 2) after intranasal administration. The extraction of main organs (lungs, spleen, liver, and kidneys) was carried out and *ex vivo* images were obtained on a Pearl® Trilogy Small Animal Imaging System.

### 2.6.2.Vaccination of mice

Six-week-old BALB/c mice were randomly separated into three groups of 4 animals and inoculated subcutaneously as follows: Group 1: Control 100 µL saline solution; Group 2: 100 µL of a solution with OmlA antigen (30 µg) plus aluminum hydroxide adjuvant (30 µg) and Group 3: 100 µL of a solution with OmlA antigen (30 µg) encapsulated into *p*NIPAM nanogels (30 µg). In all experimental groups, each mouse was inoculated following the next scheme: 0, 10, and 21 days (day 0 was defined as the first day of injections). Seven days after the last immunization (28 days) all mice were euthanized, the blood was obtained by cardiac puncture and centrifuged to obtain

serum that was stored at -20°C until further analysis. All the animal procedures were made according to Ethic Guidelines, and approved by Comité de Etica de la Investigación Cientifica (COEDI) of the Universidad Nacional de Río Cuarto (File 121/2015).

#### 2.6.2.1. ELISA (enzyme linked immunosorbent assay)

As a measure of humoral immunity, titers of IgG anti-OmlA were determined in each group according to described in Campra et al., (Campra et al., 2021). Consequently, 96-well flat-bottom polystyrene plates (Immulon 2HB) were coated with 5 µg of OmlA recombinant protein per well in a final volume of 100 µL of sodium carbonate buffer (pH 9.6) and incubated at room temperature overnight. After four washes with wash buffer (0.05% Tween 20 in PBS), the wells were blocked with 100 µL of 10% skimmed milk solution for 1 h with agitation at 37 °C. The washing procedure was carried out again and then 100 µL of mice diluted sera were added. Different dilutions were tested (1:100; 1:200; 1:400; 1:800; 1:1600; 1:3200; 1:6400; 1:10.000, 1:15.000 y 1:20.000). The plates were kept at 4°C with agitation overnight. Following the last washing, the second antibody monoclonal antibody Peroxidase AffiniPure Goat Anti-Mouse IgG (Jackson ImmunoResearch) was added and incubated for 1 h at 37 °C. At the end of the assay, and after adding 100 µL of chromogen ABTS (Azino-bis(3-ethylbenzothiazoline-6-sulfonic acid), Sigma) with 0.002% hydrogen peroxide, the OD values were measured at 405 nm using an ELISA reader (Bio-Tek Instruments, USA). The cutoff value was determined using the formula mean OD value of negative controls plus two standard deviations.

### 2.7. Statistical analyses

Statistical analyses were performed using one-way analysis of variance (ANOVA) followed by Fisher's LSD method using (SAS University Edition®) to establish differences between different experimental groups. Statistical significance was assessed as $P < 0.05$.

## 3. Results and discussion

### 3.1. Characterization of *p*NIPAM nanogels

In order to obtain the nanogel size distribution according to the thermoresponsive behavior, the hydrodynamic diameter was registered by DLS technique while the temperature of distilled water containing *p*NIPAM nanogels was modified and recorded. Average sizes of *p*NIPAM nanogels ranging from 62 to 255 nm were obtained (Figure 1A). As the results confirmed, nanogels presented thermoresponsivity showing a deswelling behavior with a significant decrease in size when the temperature increased. In Figure 1A can be clearly seen that when *p*NIPAM nanogels surpassed the phase transition temperature (Tp) at 32°C, the hydrodynamic diameter decreased

dramatically from 260 to 72 nm. The PDI remained low at all measurements as an indicator of a narrow particle size distribution (<0.3).

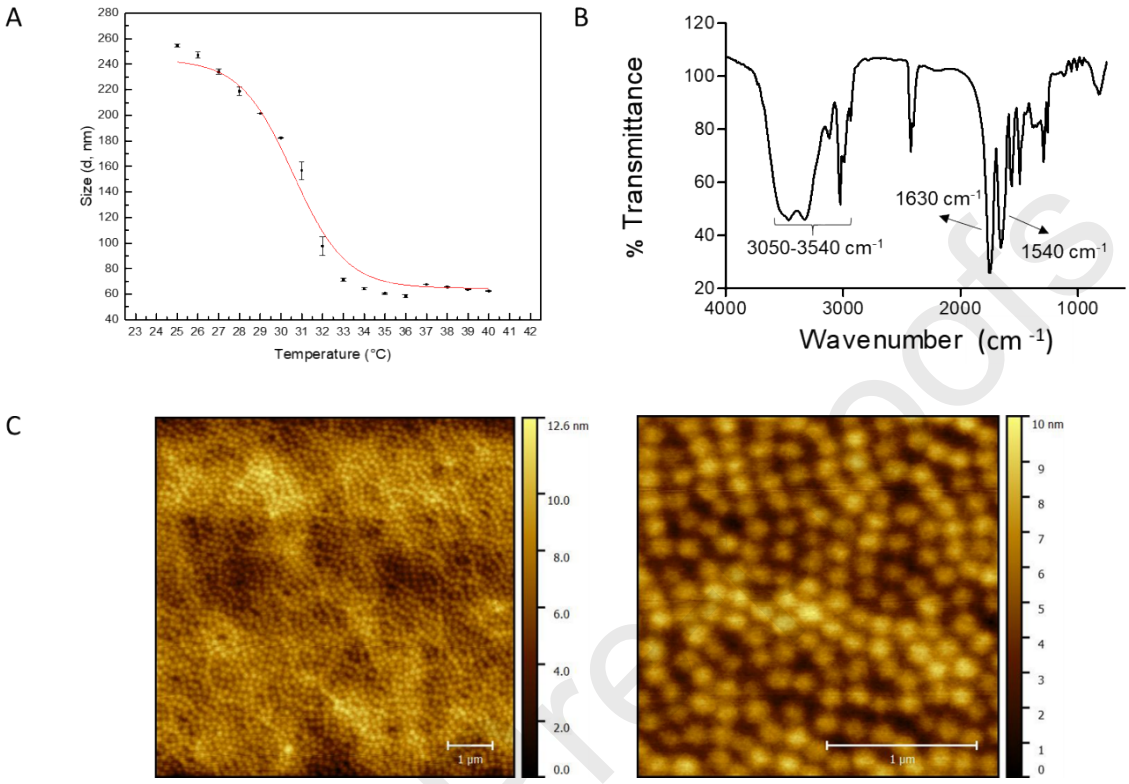


**Figure 1:** Physicochemical characterization of *p*NIPAM nanogels**. A:** Size vs temperature measure by DLS. **B**: FT-IR spectra **C**: AFM image

From the FT-IR spectrum (Figure 1B) it can be clearly recognized the characteristic bands of amide I at 1630 $cm^{-1}$ and amide II at 1540 $cm^{-1}$ correspond to NIPAM. The stretching in the region between 3050 – 3550 $cm^{-1}$ is associated with the typical elongation of overlapping of N-H and O-H functional groups (Futscher et al., 2017).

The surface topography of the nanogels was observed by AFM. The images exhibited the typical spherical shape of *p*NIPAM nanogels and their size was around 200 nm at room temperature (Figure 1C). The microphotography also showed the monodispersity of nanogels coincidently with the results of a low PDI measured by DLS.

After extensive purification by dialysis to ensure complete remotion of free dye, the covalent conjugation of FITC-nanogels was confirmed by fluorescence spectroscopy. In Figure 2 it can be observed the characteristic fluorescence emissions at 518 nm correspond to the FITC.

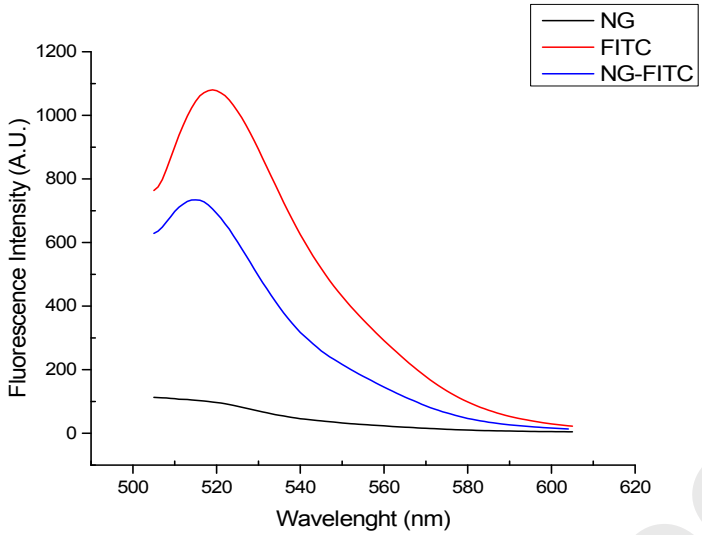


373

374 **Figure 2:** Fluorescence spectra of nanogeles, FITC and FITC-nanogels in aqueous solution

375 In a similar approach, the coupling of NIR dye on nanogels can be reflected in the corresponding
376 UV–vis spectra with an absorption peak of 805 nm produced by ADS790WS (Figure 3).

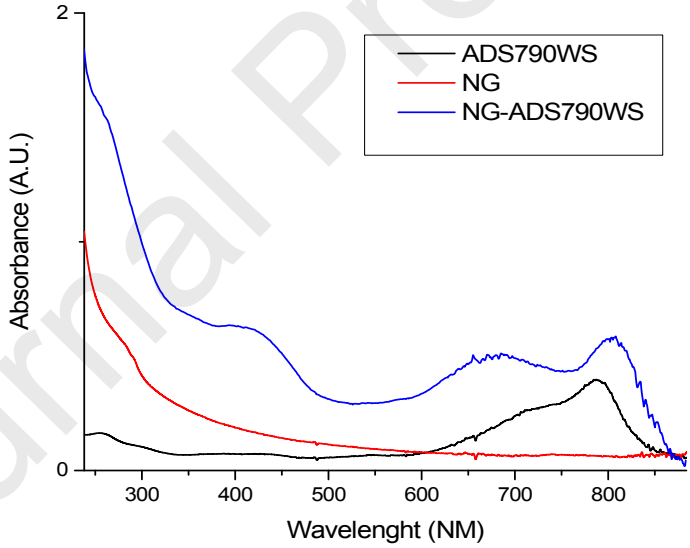


377

378 **Figure 3:** UV–VIS spectra of ADS 790 WS, nanogeles, and ADS790WS-nanogels in aqueous
379 solution

380 3.2. Expression, encapsulation and release of OmlA

381 The DNA amplicon encoding OmlA protein was correctly amplified and cloned into pGEMT Easy
382 vector, which was confirmed by restriction enzyme analysis and DNA sequencing. OmlA protein
383 was overexpressed as His-tag fusion protein, resolved in a SDS-PAGE by Coomassie staining, and

identified by Western-Blot assay using an anti-His6x primary antibody. A single band around 45-50 kDa corresponding to recombinant OmlA His-tag protein was present in the soluble fraction of total proteins (Supplementary materials 1).

The ability of nanogels to encapsulate macromolecules was tested with OmlA as an antigen and OVA as a protein model, using a 1:1 weight ratio. The OVA efficiency and capacity of loading were 97% for both. Moreover, the size for OVA-loaded nanogels was measured by DLS showing a slight increase of 7 nm after encapsulation (262 vs 255 nm for bare nanogels). The OmlA loading capacity and encapsulation efficiency calculated with this lipoprotein were both 84%. As mentioned in the literature, many factors modify the loading capacity, including the protein molecular weight and hydrophilicity. However, the resulting percentages were considered high and consistent with those obtained by Navarro and coworkers (85–98%) (Navarro et al., 2020). In the mentioned study, the OVA protein was employed and it is worth mentioning that a different crosslinking agent was used and this may generate the observed difference. As expected, the release from *p*NIPAM nanogels (Figure 4) showed a temperature dependent behavior with almost no release at 4 °C (Figure 4A), and a fast and high release of OVA and OmlA at temperatures over LCST (32 °C). The cumulative release for OmlA at 37 °C reached 65% within the first hour and 73% for OVA confirming the abrupt drug release profile of *p*NIPAM nanogels. As the results showed, nanogel swelling-deswelling behavior would provide a useful feature to be exploited for the incorporation and delivery of protein antigens in a biological system, regardless of the protein nature. Despite the collapse procedure responding to temperature changes, nanogels protected the integrity of OmlA antigen, as it was shown in SDS-PAGE analysis (Figure 4B) and OVA protein (Supplementary materials 2) noting that no proteolysis was observed. The released OmlA had the same electrophoretic profile as non-encapsulated OmlA indicating an absence of protein damage during the process. The presented bands in the gel besides that corresponding to OmlA (near the 50 kDa according to the marker line) were already observed in the anti-His6x Western-Blot assay, indicating some degraded forms of OmlA protein before encapsulation into nanogels. The mentioned protective effect was also noted in prior studies with nanogels, where encapsulated and thermo-released proteins maintained their enzymatic activity after these processes (Witting et al., 2015). The similar behavior between OVA and OmlA released at 37°C allows us to assume the same profile for retention at a standard storage temperature for vaccines.

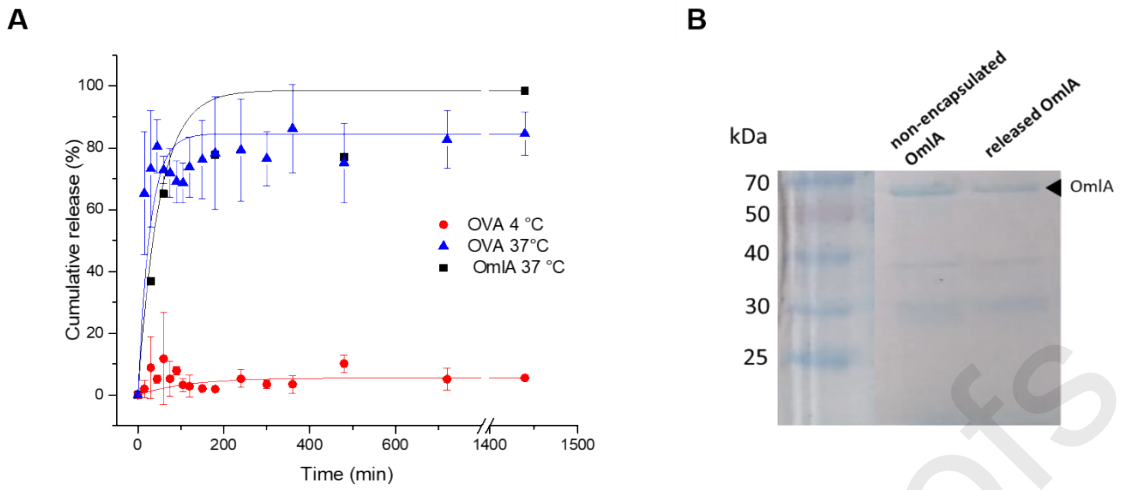


**Figure 4**: Encapsulation and release assays. **A:** *In vitro* OVA and OmlA release profile from *p*NIPAM nanogels at 4°C and 37°C. **B:** SDS-PAGE analysis of released OmlA from nanogels at 37°C compared to OmlA protein before encapsulation processes.

### 3.3. Incorporation of FITC-nanogels in macrophage cells

As FC analysis illustrated, the fluorescence intensity histograms of macrophage cells treated with FITC-nanogels were shifted to the right compared with non-treated control cells (Figure 5A). With these results, it was proven a remarkable increase in green fluorescence in RAW 264.7 cells exposed to FITC-nanogels. Quantification analysis of these histograms was performed and it could be shown that cell fluorescence intensity (represented as the geometric mean, Figure 5B) increased above the control value at 3 h of incubation time, and this cell fluorescence intensity value was maintained over the following incubation times. Interestingly, it was detected a decrease in cell fluorescence intensity at 24 h, which may be explained by the appearance of a new small cell population whit lower green fluorescence values and could be associated with a release or degradation of FITC-nanogels into the macrophages. Further studies are needed to confirm these assumptions.

These fluorescence results can be clearly interpreted due to the cell isolation and washing process that is required for subsequent cell FC analysis, and agree with the explanation provided by Rancan (Rancan et al., 2016). It is interesting to notice that 3, 6, and 12 h of incubation with FITC-nanogels had similar fluorescence intensity values which would indicate that nanogels' uptake process by RAW 264.7 cells was fast and almost completed (≈100 % cell population) at three hours. In agreement with our results, the experiments developed by Charbaji *et al*, performed with primary culture of human macrophages demonstrated an efficient particle uptake of nanogels based on *poly*-N-isopropylmethacrylamide within 3 h (Charbaji et al., 2021).

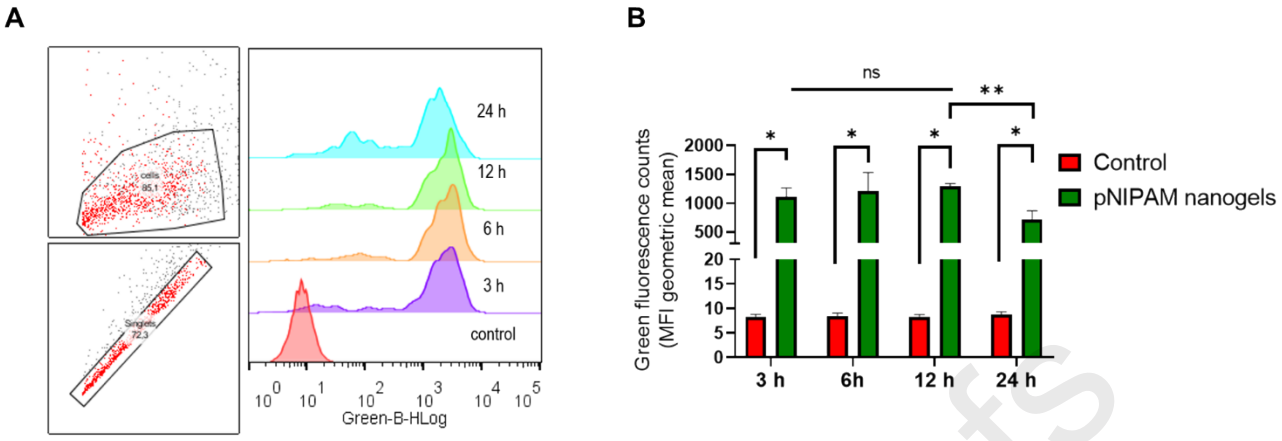


**Figure 5:** Uptake quantification of FITC-nanogels by flow cytometry in RAW 264.7 cells. **A:** Green-B-fluorescence histograms of RAW 264.7 macrophages exposed to nanogels (0.01 mg/mL) as function of cell incubation time. Beside each panel gating strategy is shown for the discrimination of singlet cells. **B:** Geometric mean fluorescence intensity of histograms shown in (A). *p ≤0.05, **p ≤ 0.001, ns= no statistically significant differences.

### 3.4. Confocal microscopy

As shown by confocal images (Figure 6), the *p*NIPAM nanogels were internalized by macrophage cells. The FITC-nanogels (green fluorescence) were observed in all macrophage cells, suggesting great incorporation into the monolayer (Figure 6A). The images confirmed the quantified data in the previous experiments analyzed by FC (Figure 5). These results are in agreement with Naha *et al*. (2010) who registered clear incorporation of *p*NIPAM nanogels by non-phagocytic human cells as HaCaT and SW480 lines (Naha et al., 2010). Also, in agreement with these authors, FITC-nanogels were exclusively observed in the cytoplasm, they did not penetrate the cell nucleus (Figure 6B). Even though, the observed pattern of green spot distribution might suggest a location in restricted areas within the lysosomes, further work is required to establish the proper location of nanogels (Figure 6B). This phenomenon has been described in numerous publications (Rancan et al., 2016), (Luckanagul et al., 2021) even with different cell cultures such as fibroblasts and dendritic cells, among others. The efficient uptake of nanosized hydrogels by mammalian cells is an important characteristic that is used in the delivery of antigens to cells of interest as APC. This process is the initial step of vaccine-induced immune responses. In our experiments, evaluated by FC and confocal imaging, murine macrophages RAW 264.7 demonstrated their capability to easily phagocyte *p*NIPAM nanogeles and located them in the cytoplasmic compartment.

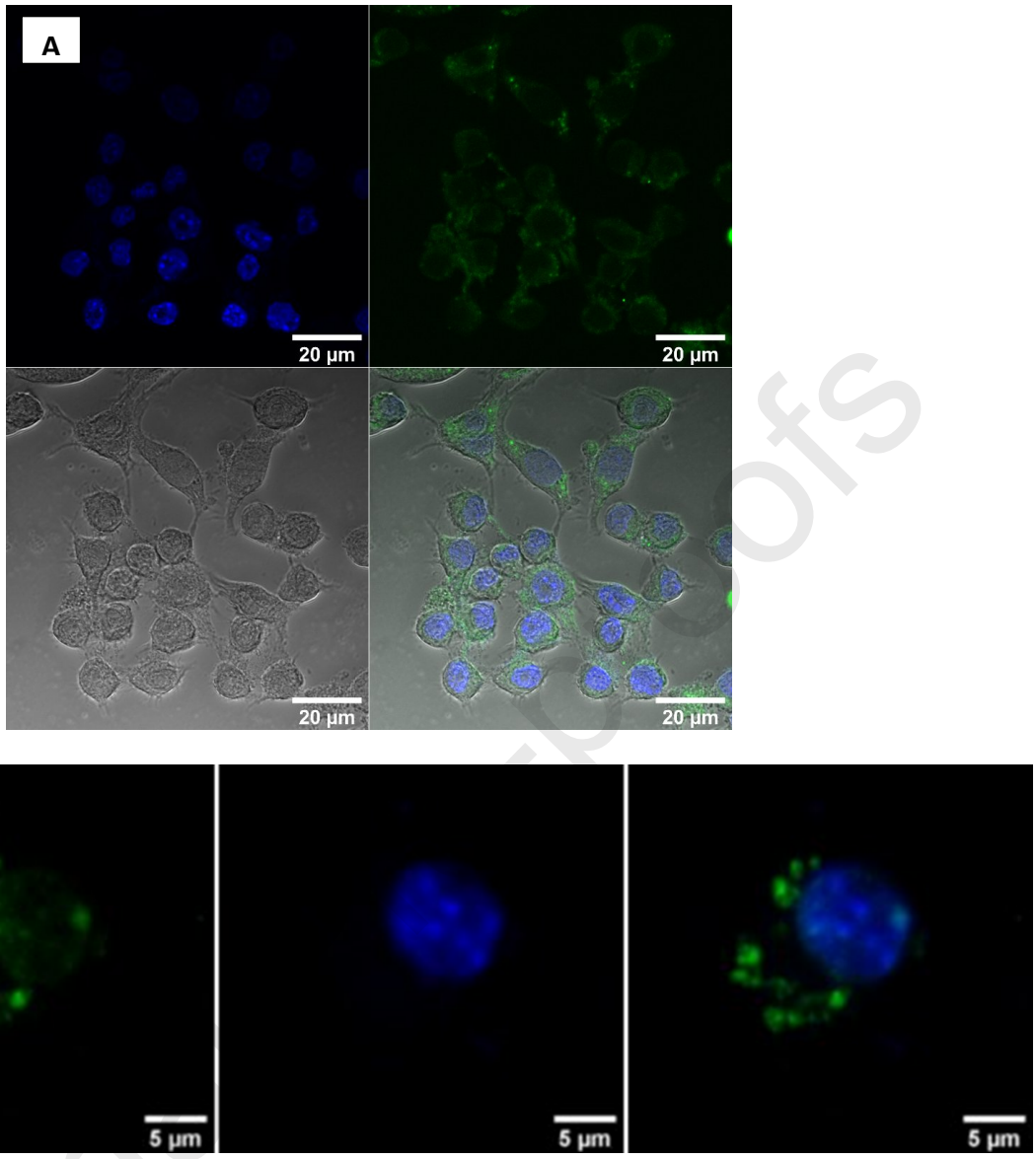


**Figure 6:** Confocal fluorescence images of *p*NIPAM nanogels internalized by RAW 264.7 macrophages after 16 h of incubation. Cell nuclei were stained with Hoechst 33342 (blue) and FITC-nanogels were visualized in green. **A:** Scale bar is 20 µm. **B:** Scale bar is 5 µm

### 3.5. Cytotoxicity assays

Following the confirmation of *p*NIPAM nanogel internalization by cells, cytotoxicity assays were conducted to evaluate the tolerance of macrophages to the nanogels cargo. First, the toxic effect of *p*NIPAM nanogels was evaluated in murine APC by MTT assay.

The MTT results showed that the averages cell viability for 0.0001 and 0.01 mg/mL *p*NIPAM nanogel concentrations were statistically similar to that of the control of untreated cells (Figure 7A), showing an absence of cell damage due to *p*NIPAM nanogel exposure. The highest nanogel

concentration (1 mg/mL), resulted in a decrease in cell survival statistically differed from negative control ($p \leq 0.05$).

The LIVE/DEAD™ Fixable Far Red cell viability assay differentiates live and dead cells using membrane integrity as a proxy for cell viability. MTT results demonstrated good biocompatibility with the macrophage cell line and the cell viability percentages for 0.0001 and 0.01 mg/mL *p*NIPAM nanogel concentrations were the same as the percentages of control cells (Figure 7B). As previously observed, 1 mg/mL nanogels concentration decreased the cell viability to 74 and 72% for 6 and 24 h respectively.

Based on these results, there was no cytotoxicity observed in response to *p*NIPAM nanogels at chosen concentrations (0.0001 and 0.01 mg/mL), except at the highest one.

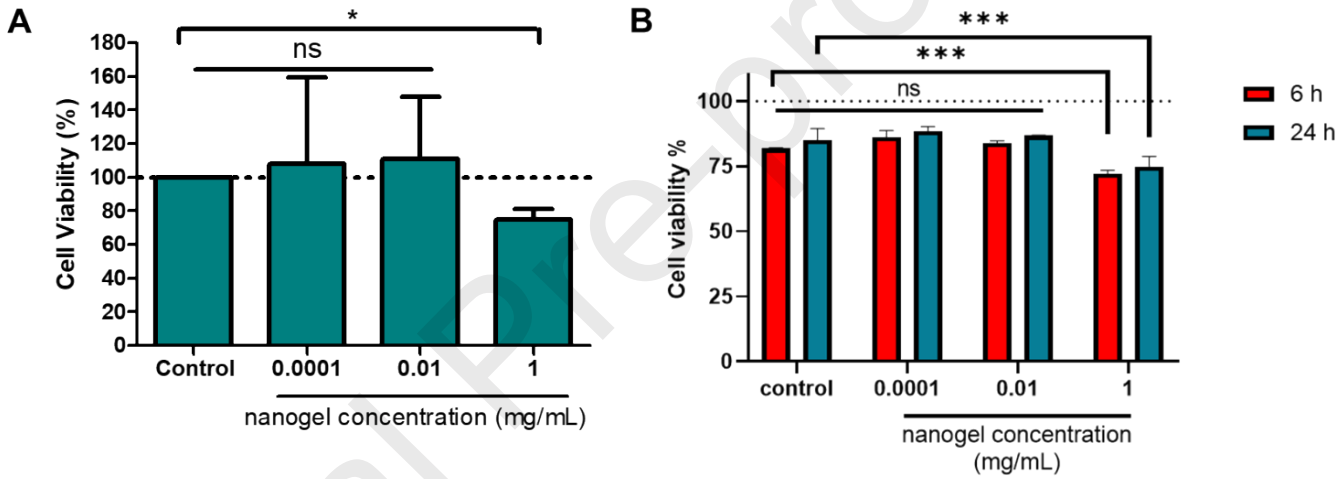


**Figure 7**: Cell viability assay in macrophages exposed to *p*NIPAM nanogels. **A**: Quantification of cell viability percentages determined by MTT assay in RAW 264.7 cell line at 24 h after nanogels incubation. **B:** Quantification of cell viability percentages by LIVE/DEAD assay in RAW 264.7 cell line at 6 and 24 h after nanogels incubation evaluated by flow cytometry. *$p \leq 0.05$, ***$p \leq 0.0001$, ns= no statistically significant differences.

### 3.6. *In vivo* imaging

The signals emitted by NIR fluorescent *p*NIPAM nanogels was correctly distinguished by Pearl® Trilogy Small Animal Imaging System (Figure 8A). All the animals remained in good general health during the experiment and no mortality was observed. The *in vivo* biodistribution of labeled nanogels is shown in Figure 8C. At basal observation (time 0), little or no signal was detected resulting in very low background fluorescence. The intranasal administration (1 mg/kg) of *p*NIPAM nanogels allowed signal detection in the mice lungs after 1 hour of inoculation, observed by *ex vivo* analysis (Figure 9A). The fluorescent signal in the lungs remained high during all evaluated periods, even at 24 h, and quantified fluorescence data confirmed an increase in the signal (Figure

9B). The presence of *p*NIPAM nanogels in the lungs had been described by Kawano in 2009 (Kawano et al., 2009). These polymeric nanoparticles were synthesized with a core-shell structure of NIPAM gel coated with gold nanorods and were systemically injected (i.v.) into mice. After 30 min, the nanoparticles accumulated in the lungs mostly, and in the liver secondly (Kawano et al. 2009). In our experiments, 4 hours after *in vivo* nanogels administration, a diffuse fluorescent signal was observed in the abdominal area indicating a systemic absorption of the nanogels (Figure 8C). The abdominal signals of *in vivo* biodistribution experiment were gradually increased and focused in the projected area of the liver after 8 hours. At 12 hours of the experiment, a stronger signal was detected in the right region of animals coinciding with the intestinal area. The images and the finding of detected fluorescent signals in feces at 12 hours suggest the elimination of nanogels through the digestive system probably through the hepatobiliary excretion pathway (Figure 8C). Fluorescent signals were predominantly detected *in vivo* and *ex vivo* in the lungs, to and lesser extent in the liver (Figure 10). The *ex vivo* quantification analysis of the main organs confirmed that little or no signal was detected in the other organs evaluated (spleen and kidneys) (Data not shown/ Supplementary materials 3). These results agree with previous studies by DeSimone (Merkel et al., 2011) that showed the circulation time and biodistribution of micrometer-sized hydrogel disks. Their results showed that softer particles could pass through lung tissue and possess longer circulation time compared with stiffer particles that were mostly entrapped in lung tissue. Moreover, Zhang et al. (Zhang et al., 2012) demonstrated that softer nanogels have longer circulation time but less splenic accumulation when compared with stiffer nanogels. Contrary to these findings, Schlachet *et al*. observed an important brain and head accumulation of mixed amphiphilic nanoparticles made of chitosan-g-poly(methyl methacrylate) and poly(vinyl alcohol)-g-poly(methyl methacrylate) after intranasal application in mice (Schlachet et al., 2020). The inoculation was made to improve drug bioavailability in the brain, using 20 µL per mouse. The average size of nanoparticles was similar to *p*NIPAM nanogels (around 200 nm) at environmental temperature, and they could distinguish the nanogels presence in other organs like the spleen and heart, among others. The accumulation of nanogels was taken place in the lungs first, and in the liver secondly. The contrasting results in the bibliography about nanoparticle biodistribution, including our results, emphasize the importance of verifying each nanoplatform performance.

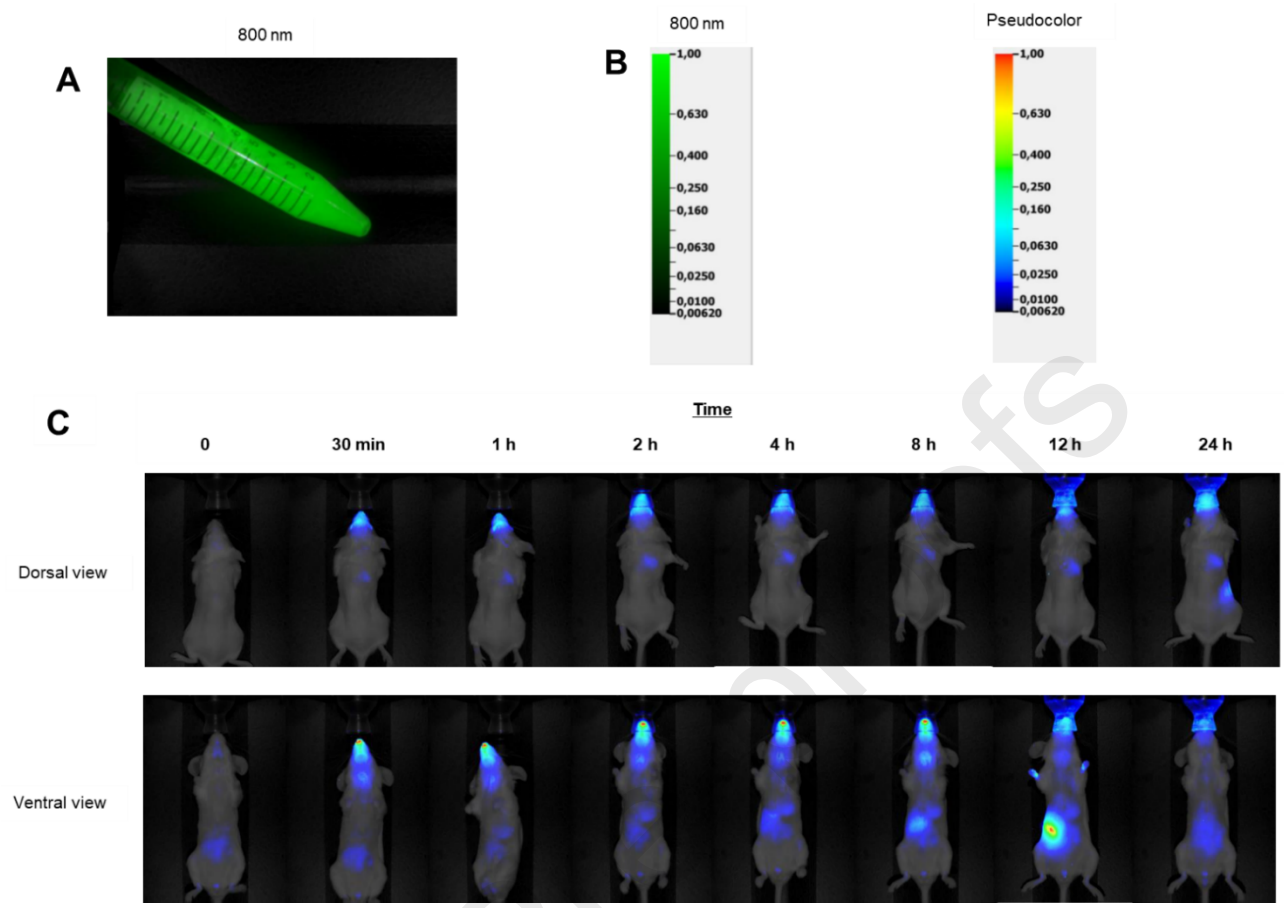


537

538 **Figure 8: A:** Image of *p*NIPAM nanogels labeled with ADS790WS IR dye at 800 nm **B:** Scale used for 800
539 nm and for the generation of pseudocolor images. **C:** Representative images acquired at different times
540 of dorsal and ventral view in pseudocolor of mice administered intranasally with ADS790WS-nanogels.

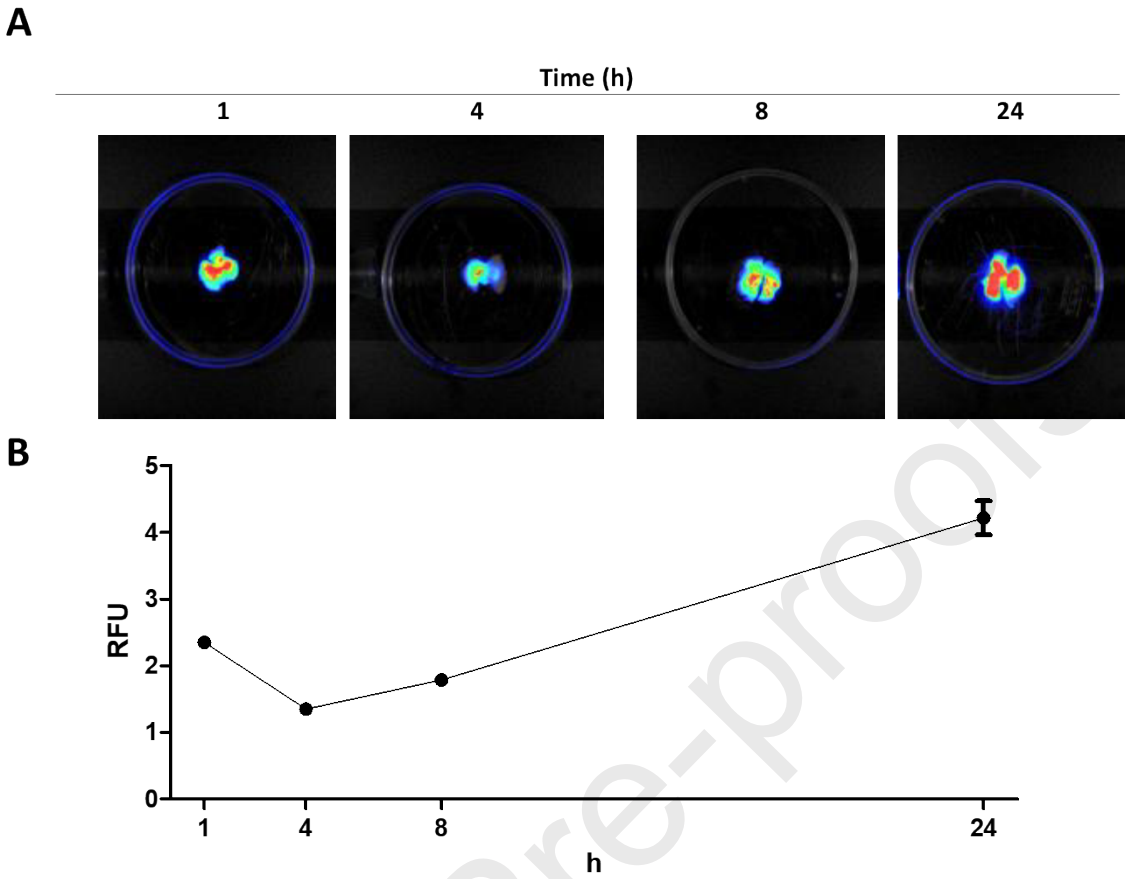


**Figure 9:** Fluorescence analysis of lungs in mice administered intranasally with ADS79WS-nanogels. **A:** Representative *ex vivo* fluorescence images of lungs at different times in pseudocolor mode. **B:** Quantitative analysis of fluorescence of lungs (RFU: relative fluorescence units). Data are presented as mean ± standard deviations

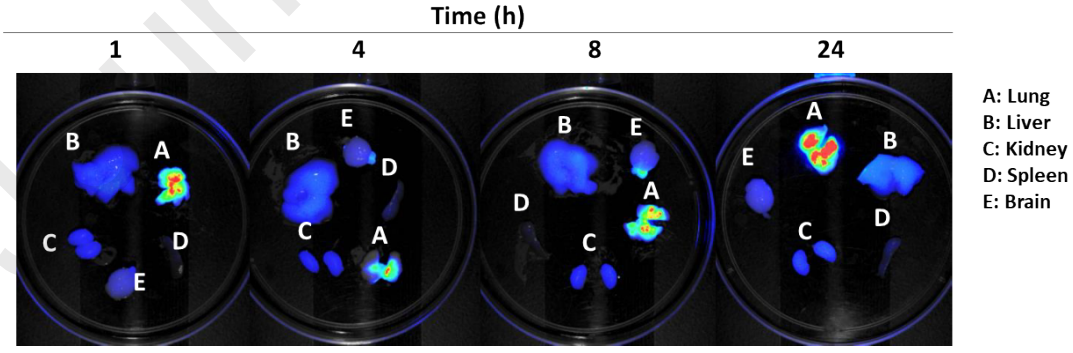


**Figure 10:** Fluorescence analysis of organs in mice administered intranasally with ADS790WS-nanogels. Representative *ex vivo* fluorescence images of lungs, liver, kidneys and spleen, and brain in pseudocolor mode

552 3.7. ELISA (enzyme linked immunosorbent assay)

553 A considerable amount of literature has been published on vaccines based on nanogels to develop
554 a new prophylactic strategy, even in veterinary medicine (Debache et al., 2011; Yang et al., 2017).
555 The use of classical adjuvants such as aluminum hydroxide or Freund´s adjuvants in the
556 experimental model is a common tool to compare the performance of nanogels as a vaccine
557 adjuvant (Li et al., 2013). Traditional adjuvant action is frequently associated with an increase of
558 local toxicity, which triggers an inflammatory reaction in the inoculation tissue. Therefore, there
559 is a need for alternatives with less toxicity.

560 In this work, the potential antigen delivery function of nanogels was further investigated in mice
561 using OmlA protein, a bacterial virulence factor of *Actinobacillus pleuropneumoniae*. For this, the
562 antigen was mixed with nanogels or aluminum hydroxide adjuvant to generate the experimental
563 vaccine formulations. As Figure 11 shows, it was observed that the titer of OmlA-specific IgG
564 antibodies was the same in mice injected with the OmlA-nanogels as in those inoculated with the
565 OmlA-aluminum hydroxide adjuvant. Both cases had the same antibody titers in serum, reaching
566 1:6400. These antibody titers suggest the ability of nanogels to stimulate a humoral immune
567 response. It is interesting to note that this positive effect on immune response was produced in
568 absence of cell damage, even with the confirmation of the nanogels intracellular localization
569 assays. The main advantage of nanogels is that they show the same efficacy with less toxicity.
570 Anyway, other complimentary assays must be performed to understand the interaction between
571 nanogels and APC.

572 Although extensive research on nanogels has been successfully carried out, the action of each
573 nanogels-based system needs to be described due to the numerous immune response modifying
574 factors. Shakya et al. 2011, described the adjuvant properties of N-isopropylacrylamide polymer
575 (Shakya et al., 2011). However, it is not a recently published article and they did not use
576 nanoparticles, there are interesting findings to highlight about the studied material. The author
577 observed similar antibody levels in mice vaccinated with *p*NIPAM with collagen type II (CII)
578 (elected antigen) compare to complete Freund´s adjuvant with CII protein. The findings were
579 better in the case of physically entrapped than for the covalent coupling of antigen, and the
580 antibody response recognized the native form of CII. The latter is consistent with the protective
581 effect of *p*NIPAM nanogels found on the loaded and released OmlA antigen.

582

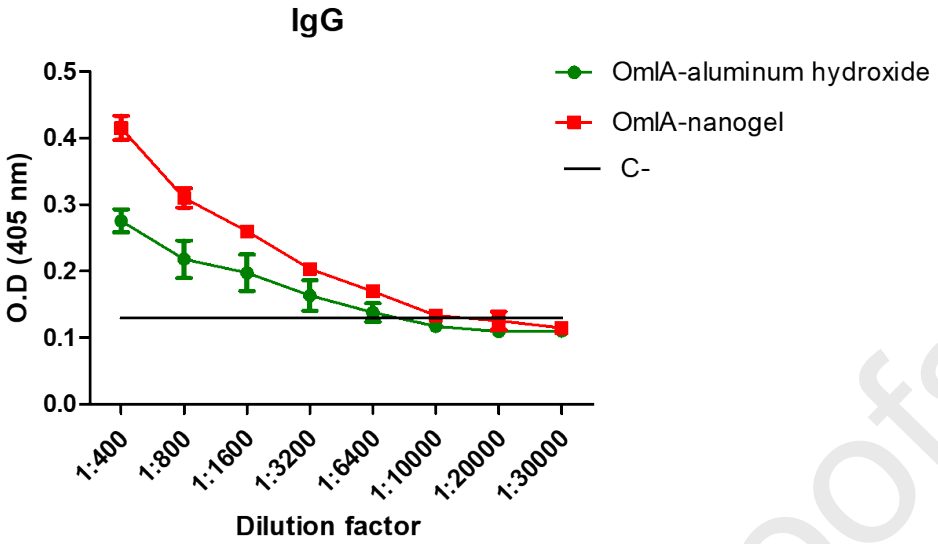


583

584 **Figure 11:** Specific humoral immune response in serum by ELISA. Each point represents geometric mean
585 of optical density value (n=4) according to the dilution factors used. The mean of negative control plus 2
586 standard deviations, was considered as negative cut-off (C-) (black line)

587

588 ## 4. Conclusion

589 In the present work, nanogels based on *p*NIPAM were obtained by precipitation polymerization
590 and tested as vaccine nanocarriers. Their physicochemical characterization and their "smart"
591 ability to transport, protect and release the OmlA antigen lipoprotein were proved. In this work,
592 the first steps to a successful immune response were obtained with *p*NIPAM nanogels, since they
593 were incorporated in a model of APC (RAW 264.7) within three hours without evidence of
594 cytotoxic damage in cell culture. The response of BALB/c mice vaccinated with OmlA-nanogels
595 formulation was adequate, taking into account that the anti- OmlA IgG titer was equal to the
596 conventional aluminum hydroxide adjuvant formulation. The utilization of *p*NIPAM nanogel-
597 based vaccines for mucosal immunization might have advantages over other classical adjuvants
598 given that *in vivo* imaging results on biodistribution show that fluorescent signals were
599 predominantly detected in the lungs when nanogels were administered intranasally. The results
600 obtained from these preliminary studies summarize an excellent biocompatible alternative to
601 choose in new formulations of vaccines for mucosal application.

602 ## Conflicts of interest

603 There are no conflicts to declare. The authors declare no competing financial interest.

604 ## Acknowledgements

605 We gratefully acknowledge financial support from CONICET, FONCyT (PICT 2018-03338, PICT
606 2017-2180, PICT 2019-02450) INTA (I102 project), and SeCyT-UNRC. We acknowledge Ulises

607 Notario for the *in vivo* biodistribution images. M.L. Soriano Perez and C. Flores thanks CONICET
608 for a graduate research fellowship.

609 Author Credit Statement: M.L. Soriano Perez: Conceptualization, Methodology, Formal analysis,
610 Investigation, Writing - Original Draft, Writing - review & editing; J. Funes: Investigation; C. Flores:
611 Investigation; L. Ibarra: Investigation, Writing - review & editing; M.A. Forrellad: Investigation,
612 Writing - review & editing; O. Taboga: Investigation, Formal analysis; L.N. Cariddi: Investigation ,
613 Writing - review & editing; F. Salinas: Investigation; H.H. Ortega: Methodology, Formal analysis ,
614 Writing - review & editing; F. Alustiza: Conceptualization, Methodology, Writing - Original Draft,
615 Writing - review & editing, Supervision, Funding acquisition; M. Molina: Conceptualization,
616 Writing - Original Draft, Writing - review & editing, Supervision, Funding acquisition.

617

618

## References


Alcón, V., Baca-Estrada, M., Vega-Lopez, M., Willson, P., Babiuk, L.A., Kumar, P., Hecker, R., Foldvari, M., 2006. Mucosal delivery of bacterial antigens and CpG oligonucleotides formulated in biphasic lipid vesicles in pigs. AAPS J. 7, E566–E571. https://doi.org/10.1208/aapsj070357

Alcón, V.L., Baca-Estrada, M., Vega-López, M.A., Willson, P., Babiuk, L.A., Kumar, P., Foldvari, M., 2005. Intranasal immunization using biphasic lipid vesicles as delivery systems for OmlA bacterial protein antigen and CpG oligonucleotides adjuvant in a mouse model. J. Pharm. Pharmacol. 57, 955–961. https://doi.org/10.1211/0022357056695

Alcón, V.L., Foldvari, M., Snider, M., Willson, P., Gomis, S., Hecker, R., Babiuk, L.A., Baca-Estrada, M.E., 2003. Induction of protective immunity in pigs after immunisation with CpG oligodeoxynucleotides formulated in a lipid-based delivery system (Biphasix™). Vaccine 21, 1811–1814. https://doi.org/10.1016/S0264-410X(03)00003-3

Boutris, C., Chatzi, E.G., Kiparissides, C., 1997. Characterization of the LCST behaviour of aqueous poly(N-isopropylacrylamide) solutions by thermal and cloud point techniques. Polymer (Guildf). 38, 2567–2570. https://doi.org/10.1016/S0032-3861(97)01024-0

Campra, N.A., Montironi, I.D., Reinoso, E.B., Raviolo, J., Moreno, F.R., Maletto, B., Cariddi, L.N., 2021. A natural oil increases specific anti-OVA IgG levels and induces a cellular immune response combined with aluminum hydroxide. J. Leukoc. Biol. 109, 223–232. https://doi.org/10.1002/JLB.3AB0720-093RR

Carvalho, S.G., Araujo, V.H.S., dos Santos, A.M., Duarte, J.L., Silvestre, A.L.P., Fonseca-Santos, B., Villanova, J.C.O., Gremião, M.P.D., Chorilli, M., 2020. Advances and challenges in nanocarriers and nanomedicines for veterinary application. Int. J. Pharm. 580, 119214. https://doi.org/10.1016/j.ijpharm.2020.119214

Chacko, R.T., Ventura, J., Zhuang, J., Thayumanavan, S., 2012. Polymer nanogels: A versatile nanoscopic drug delivery platform. Adv. Drug Deliv. Rev. 64, 836–851. https://doi.org/10.1016/j.addr.2012.02.002

Chalal, M., Ehrburger-Dolle, F., Morfin, I., Bley, F., Aguilar De Armas, M.R., López Donaire, M.L., San Roman, J., Bölgen, N., Pişkin, E., Ziane, O., Casalegno, R., 2010. SAXS investigation of the effect of temperature on the multiscale structure of a macroporous poly(N-isopropylacrylamide) gel. Macromolecules 43, 2009–2017. https://doi.org/10.1021/ma902655h

651 Charbaji, R., Kar, M., Theune, L.E., Bergueiro, J., Eichhorst, A., Navarro, L., Graff, P., Stumpff, F.,
652 Calderón, M., Hedtrich, S., 2021. Design and Testing of Efficient Mucus-Penetrating
653 Nanogels—Pitfalls of Preclinical Testing and Lessons Learned. Small 17, 1–17.
654 https://doi.org/10.1002/smll.202007963

655 Debache, K., Kropf, C., Schütz, C.A., Harwood, L.J., Käuper, P., Monney, T., Rossi, N., Laue, C.,
656 Mccullough, K.C., Hemphill, A., 2011. Vaccination of mice with chitosan nanogel-
657 associated recombinant NcPDI against challenge infection with Neospora caninum
658 tachyzoites. Parasite Immunol. 33, 81–94. https://doi.org/10.1111/j.1365-
659 3024.2010.01255.x

660 Futscher, M.H., Philipp, M., Müller-Buschbaum, P., Schulte, A., 2017. The Role of Backbone
661 Hydration of Poly(N-isopropyl acrylamide) Across the Volume Phase Transition Compared
662 to its Monomer. Sci. Rep. 7. https://doi.org/10.1038/s41598-017-17272-7

663 Gottschalk, M., 2012. Actinobacillosis, in: Zimmerman, J.J., Karriker, L.A., Ramirez, A., Schwartz,
664 K.J., Stevenson, G.W. (Eds.), Diseases of Swine. Wiley-Blackwell.

665 Hernández-Adame, L., Angulo, C., García-Silva, I., Palestino, G., Rosales-Mendoza, S., 2019. An
666 overview of nanogel-based vaccines. Expert Rev. Vaccines 18, 951–968.
667 https://doi.org/10.1080/14760584.2019.1647783

668 Kawano, T., Niidome, Y., Mori, T., Katayama, Y., Niidome, T., 2009. PNIPAM gel-coated gold
669 nanorods for targeted delivery responding to a near-infrared laser. Bioconjug. Chem. 20,
670 209–212. https://doi.org/10.1021/bc800480k

671 Li, P., Luo, Z., Liu, P., Gao, N., Zhang, Y., Pan, H., Liu, L., Wang, C., Cai, L., Ma, Y., 2013.
672 Bioreducible alginate-poly(ethylenimine) nanogels as an antigen-delivery system robustly
673 enhance vaccine-elicited humoral and cellular immune responses. J. Control. Release 168,
674 271–279. https://doi.org/10.1016/j.jconrel.2013.03.025

675 Loera-Muro, A., Angulo, C., 2018. New trends in innovative vaccine development against
676 Actinobacillus pleuropneumoniae. Vet. Microbiol.
677 https://doi.org/10.1016/j.vetmic.2018.02.028

678 Luckanagul, J.A., Bhuket, P.R.N., Muangnoi, C., Rojsitthisak, Pranee, Wang, Q., Rojsitthisak,
679 Pornchai, 2021. Self-assembled thermoresponsive nanogel from grafted hyaluronic acid as
680 a biocompatible delivery platform for curcumin with enhanced drug loading and biological
681 activities. Polymers (Basel). 13, 1–14. https://doi.org/10.3390/polym13020194

682 Merkel, T.J., Jones, S.W., Herlihy, K.P., Kersey, F.R., Shields, A.R., Napier, M., Luft, J.C., Wu, H.,

683 Zamboni, W.C., Wang, A.Z., Bear, J.E., DeSimone, J.M., 2011. Using mechanobiological
684 mimicry of red blood cells to extend circulation times of hydrogel microparticles. Proc.
685 Natl. Acad. Sci. U. S. A. 108, 586–591. https://doi.org/10.1073/pnas.1010013108

686 Molina, M., Asadian-Birjand, M., Balach, J., Bergueiro, J., Miceli, E., Calderón, M., 2015. Stimuli-
687 responsive nanogel composites and their application in nanomedicine. Chem. Soc. Rev. 44,
688 6161–6186. https://doi.org/10.1039/c5cs00199d

689 Naha, P.C., Bhattacharya, K., Tenuta, T., Dawson, K.A., Lynch, I., Gracia, A., Lyng, F.M., Byrne,
690 H.J., 2010. Intracellular localisation, geno- and cytotoxic response of polyN-
691 isopropylacrylamide (PNIPAM) nanoparticles to human keratinocyte (HaCaT) and colon
692 cells (SW 480). Toxicol. Lett. 198, 134–143. https://doi.org/10.1016/j.toxlet.2010.06.011

693 Navarro, L., Theune, L.E., Calderón, M., 2020. Effect of crosslinking density on thermoresponsive
694 nanogels: A study on the size control and the kinetics release of biomacromolecules. Eur.
695 Polym. J. 124, 109478. https://doi.org/10.1016/j.eurpolymj.2020.109478

696 Neamtu, I., Rusu, A.G., Diaconu, A., Nita, L.E., Chiriac, A.P., 2017. Basic concepts and recent
697 advances in nanogels as carriers for medical applications. Drug Deliv. 24, 539–557.
698 https://doi.org/10.1080/10717544.2016.1276232

699 Nochi, T., Yuki, Y., Takahashi, H., Sawada, S.I., Mejima, M., Kohda, T., Harada, N., Kong, I.G., Sato,
700 A., Kataoka, N., Tokuhara, D., Kurokawa, S., Takahashi, Y., Tsukada, H., Kozaki, S., Akiyoshi,
701 K., Kiyono, H., 2010. Nanogel antigenic protein-delivery system for adjuvant-free intranasal
702 vaccines. Nat. Mater. 9, 572–578. https://doi.org/10.1038/nmat2784

703 Pelton, R.H., Chibante, P., 1986. Preparation of aqueous latices with N-isopropylacrylamide.
704 Colloids and Surfaces 20, 247–256. https://doi.org/10.1016/0166-6622(86)80274-8

705 Pippa, N., Gazouli, M., Pispas, S., 2021. Recent advances and future perspectives in
706 polymer-based nanovaccines. Vaccines 9, 1–20. https://doi.org/10.3390/vaccines9060558

707 Preman, N.K., Barki, R.R., Vijayan, A., Sanjeeva, S.G., Johnson, R.P., 2020. Recent developments
708 in stimuli-responsive polymer nanogels for drug delivery and diagnostics: A review. Eur. J.
709 Pharm. Biopharm. 157, 121–153. https://doi.org/10.1016/j.ejpb.2020.10.009

710 Rancan, F., Asadian-Birjand, M., Dogan, S., Graf, C., Cuellar, L., Lommatzsch, S., Blume-Peytavi,
711 U., Calderón, M., Vogt, A., 2016. Effects of thermoresponsivity and softness on skin
712 penetration and cellular uptake of polyglycerol-based nanogels. J. Control. Release 228,
713 159–169. https://doi.org/10.1016/j.jconrel.2016.02.047

714 Schlachet, I., Halamish, H.M., Sosnik, A., 2020. Mixed amphiphilic polymeric nanoparticles of

chitosan, poly(vinyl alcohol) and poly(methyl methacrylate) for intranasal drug delivery: A preliminary in vivo study. Molecules 25. https://doi.org/10.3390/molecules25194496

Shakya, A.K., Kumar, A., Nandakumar, K.S., 2011. Adjuvant properties of a biocompatible thermo-responsive polymer of N-isopropylacrylamide in autoimmunity and arthritis. J. R. Soc. Interface 8, 1748–1759. https://doi.org/10.1098/rsif.2011.0114

Tang, L., Wang, L., Yang, X., Feng, Y., Li, Y., Feng, W., 2021. Poly(N-isopropylacrylamide)-based smart hydrogels: Design, properties and applications. Prog. Mater. Sci. 115. https://doi.org/10.1016/j.pmatsci.2020.100702

Tokuhiro, T., Amiya, T., Mamada, A., Tanaka, T., 1991. NMR Study of PolytN-isopropylacrylamide ) Gels Transition Phase 2936–2943.

Wibowo, D., Jorritsma, S.H.T., Gonzaga, Z.J., Evert, B., Chen, S., Rehm, B.H.A., 2021. Polymeric nanoparticle vaccines to combat emerging and pandemic threats. Biomaterials 268, 120597. https://doi.org/10.1016/j.biomaterials.2020.120597

Witting, M., Molina, M., Obst, K., Plank, R., Eckl, K.M., Hennies, H.C., Calderón, M., Frieß, W., Hedtrich, S., 2015. Thermosensitive dendritic polyglycerol-based nanogels for cutaneous delivery of biomacromolecules. Nanomedicine Nanotechnology, Biol. Med. 11, 1179–1187. https://doi.org/10.1016/j.nano.2015.02.017

Yang, J., Shim, S.M., Nguyen, T.Q., Kim, E.H., Kim, K., Lim, Y.T., Sung, M.H., Webby, R., Poo, H., 2017. Poly-Î 3-glutamic acid/chitosan nanogel greatly enhances the efficacy and heterosubtypic cross-reactivity of H1N1 pandemic influenza vaccine. Sci. Rep. 7, 1–14. https://doi.org/10.1038/srep44839

Zhang, L., Cao, Z., Li, Y., Ella-Menye, J.R., Bai, T., Jiang, S., 2012. Softer zwitterionic nanogels for longer circulation and lower splenic accumulation. ACS Nano 6, 6681–6686. https://doi.org/10.1021/nn301159a

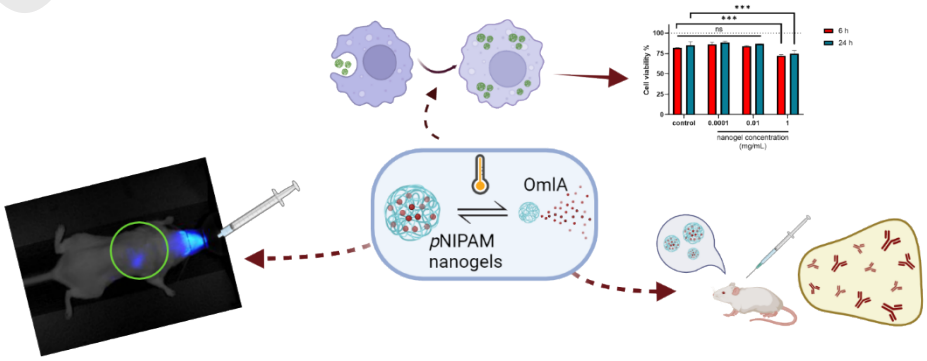

Highlights

- Thermoresponsive nanogeles are developed as vaccine platform
- Nanogels are internalized by macrophage cell line in absence of cytotoxicity
- Fluorescence of nanogels is detected in faeces after intranasal inoculation in mice
- OmlA-nanogels formulation produces detectable titer of OmlA-specific IgG antibodies

Author Credit Statement: M.L. Soriano Perez: Conceptualization, Methodology, Formal analysis, Investigation, Writing - Original Draft, Writing - review & editing; J. Funes: Investigation; C. Flores: Investigation; L. Ibarra: Investigation, Writing - review & editing; M.A. Forrellad: Investigation, Writing - review & editing; O. Taboga: Investigation, Formal analysis; L.N. Cariddi: Investigation , Writing - review & editing; F. Salinas: Investigation; H.H. Ortega: Methodology, Formal analysis , Writing - review & editing; F. Alustiza: Conceptualization, Methodology, Writing - Original Draft, Writing - review & editing, Supervision, Funding acquisition; M. Molina: Conceptualization, Writing - Original Draft, Writing - review & editing, Supervision, Funding acquisition.

**Declaration of interests**

☒ The authors declare that they have no known competing financial interests or personal relationships that could have appeared to influence the work reported in this paper.

☐ The authors declare the following financial interests/personal relationships which may be considered as potential competing interests: